Analyzing Seismocardiogram Cycles to Identify the Respiratory Phases

Vahid Zakeri*, *Member, IEEE*, Alireza Akhbardeh, Nasim Alamdari, Reza Fazel-Rezai, *Senior Member, IEEE*, Mikko Paukkunen, and Kouhyar Tavakolian

***Abstract*—*Goal:* the objective of this study was to develop a method to identify respiratory phases (i.e., inhale or exhale) of seismocardiogram (SCG) cycles. An SCG signal is obtained by placing an accelerometer on the sternum to capture cardiac vibrations. *Methods:* SCGs from 19 healthy subjects were collected, preprocessed, segmented, and labeled. To extract the most important features, each SCG cycle was divided to equal-sized bins in time and frequency domains, and the average value of each bin was defined as a feature. Support vector machines was employed for feature selection and identification. The features were selected based on the total accuracy. The identification was performed in two scenarios: leave-one-subject-out (LOSO), and subject-specific (SS). *Results:* time-domain features resulted in better performance. The time-domain features that had higher accuracies included the characteristic points correlated with aortic-valve opening, aortic-valve closure, and the length of cardiac cycle. The average total identification accuracies were 88.1% and 95.4% for LOSO and SS scenarios, respectively. *Conclusion:* the proposed method was an efficient, reliable, and accurate approach to identify the respiratory phases of SCG cycles. *Significance:* The results obtained from this study can be employed to enhance the extraction of clinically valuable information such as systolic time intervals.**

***Index Terms*—Respiratory phase identification, seismocardiogram (SCG), support vector machine (SVM), systolic time intervals (STI).**

I. Introduction

CARDIAC activities create vibrations that are transmitted to the chest wall. Such vibrations can be captured noninvasively by placing an accelerometer on the sternum. The captured signal is called seismocardiogram (SCG) [1]–[3]. The availability of modern, high-quality, and inexpensive accelerometers combined with improving low-cost computational power allows SCG to be recorded and analyzed quickly and efficiently [4].

Analyzing SCG has revealed valuable clinical information about cardiac activities such as myocardial contractility and systolic time intervals (STI). Myocardial contractility, which indicates the ability of heart muscles to contract, can be invasively assessed by using catheters to measure the pressure change in the left ventricle [4]. SCG can be used for noninvasive assessment of myocardial contractility [3], [5], [6]. Moreover, STI provide a quantitative estimation for left ventricle performance in the presence of cardiovascular disorders [7].

Crow *et al.* compared SCG with echocardiography (Echo), cardiology's gold standard, and indicated specific SCG points that could be used for estimating STI. They concluded that because of the consistency between SCG and Echo points, they were equally accurate in measuring STI [8]. SCG has been used in recent studies to extract different STI such as pre-ejection period, left ventricular ejection time, and electromechanical systole (QS2) [6], [9]–[13].

In addition to cardiac information, SCG contains respiratory information, as it can capture the movements of the chest due to respiratory expansion and contraction of lungs [14]. As a result, SCG can also be employed in respiratory assessment. For instance, it has been used for estimating respiratory rate [15] and screening for sleep apnea [16].

However, respiration affects SCG signals. Tavakolian *et al.* indicated that SCG cycles corresponding to inhale and exhale phases of respiration have different morphologies. This finding was used to improve the signal averaging [17]. In another study, Pandia *et al.* extracted specific respiration-dependent features of SCG including amplitude and timing changes within and between heartbeats [14].

Considering the respiratory effects on morphology, amplitude, and timing of SCG signals, relevant cardiac information such as STI can be significantly different in different respiration phases. That is, SCG beat-to-beat cycles corresponding to inhale are different from those corresponding to exhale, as shown in Fig. 1. Therefore, it is necessary to differentiate SCG cycles based on their position in the respiratory phases.

The focus of this study was to develop an algorithm that can identify the respiratory phases of SCG cycles without an independent recording of the respiration signal, as this imposes extra complexity and cost.

Manuscript received August 2, 2016; revised September 23, 2016; accepted October 18, 2016. Date of publication October 26, 2016; date of current version July 15, 2017. This work was supported in part by the Industrial R&D Fellowship of Natural Sciences and Engineering Research Council of Canada. *Asterisk indicates corresponding author.*

*V. Zakeri was with the Heart Force Medical Inc., Vancouver, BC V6C 3P6, Canada. He is now with the Department of Mechanical Engineering, University of British Columbia, Vancouver, BC V6T 1Z4, Canada (e-mail: vahid.zakeri@mech.ubc.ca).

A. Akhbardeh is with the School of Medicine, Johns Hopkins University.

N. Alamdari, R. Fazel-Rezai, and K. Tavakolian are with the Department of Electrical Engineering, University of North Dakota.

M. Paukkunen is with the Department of Electrical Engineering and Automation, Aalto University.

Digital Object Identifier 10.1109/TBME.2016.2621037

0018-9294 © 2016 Canadian Crown Copyright

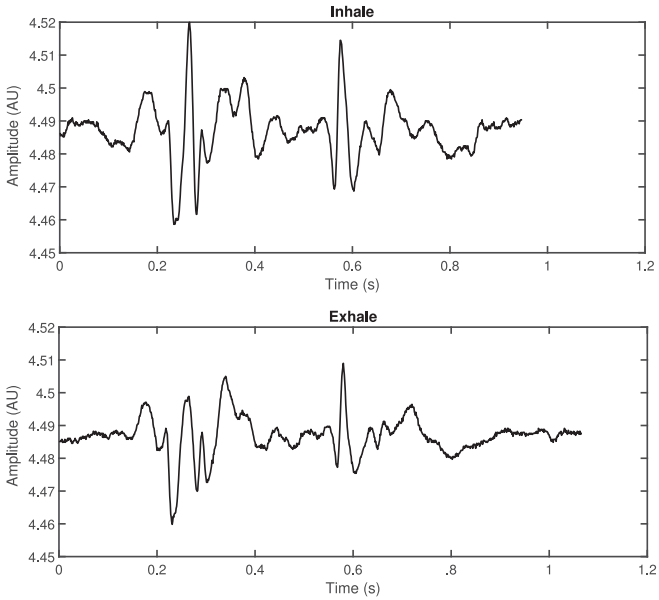

Fig. 1. SCG cycles in inhale (top) and exhale (bottom) phases obtained from one subject.

There exist a body of work using electrocardiogram (ECG) or SCG to extract respiratory information such as respiration rate, but none of them have investigated the phase identification of cardiac cycles [18]–[21]. The closest work to this study was done by Alamdari *et al.*, in which an envelope detection method was employed on SCG to derive the respiration signal [22]. The respiratory phases of SCG cycles were identified using the derived respiration signal. Such analysis involved delays between the derived signal and the measured respiratory belt signal. Moreover, prior knowledge was needed as to whether to choose the upper or the lower envelope of SCG signal.

In another work, Pandia *et al.* performed a frequency domain analysis on SCG in the range 0–100 Hz [23]. They subdivided this range into 5 and 10 Hz frequency bins and indicated a statistically significant difference between the power of inspiratory and expiratory SCG cycles in 10–40 Hz range. Despite the results, no classification or identification among SCG cycles was conducted in their study.

This paper presents a novel method for identifying the respiratory phases of SCG cycles. Our approach is based on machine-learning techniques [24]; a preliminary version of the study has been reported [25]. Section II outlines the methodology, Section III shows the results, Section IV contains discussions, and Section V provides conclusions.

II. Methodology

A. Data Collection and Preprocessing

Ethics approval was given by Aalto University, Finland for this study, and consent was received from 20 healthy male subjects with no known history of cardiovascular or pulmonary diseases (age: 24.8 ± 3.09 years; height: 180.6 ± 5.10 cm; weight: 78.9 ± 9.05 kg). The trial was performed twice for each subject, and each trial took about 10 min with 1000-Hz sampling frequency (total 40 trials).

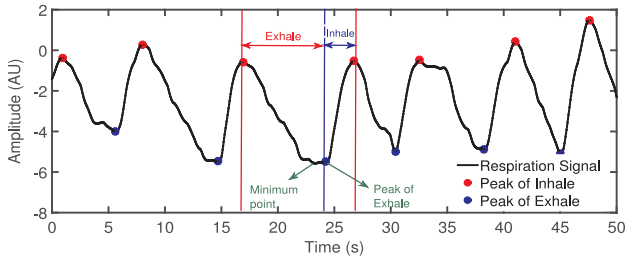

Fig. 2. Manual annotation of the respiration signal.

A respiration belt sensor (BN-RESP-XDCR, BIOPAC Systems Inc., Goleta, CA, USA) was used to measure the respiration signal (effort). The belt sensor was tightened around the chest to record breathing properly. A three-component accelerometer (SCA610-C21H1A, VTI Technologies, Vantaa, Finland) was mounted on the sternum using double-sided adhesive tape along the *x*-, *y*-, and *z*-axes. The accelerometer sensor was placed about one centimeter above the xyphoid process.

The rated frequency response of the accelerometers was 50 ± 30 Hz. The input range was ± 1 g. The accelerometer was separately measured at the manufacturer's laboratory and was shown to have a cutoff frequency (– 3 dB) at 46 Hz. To reduce high-frequency noise and provide antialias filtering, the accelerometer output was fed through an eigth-order Bessel low-pass filter before analog-to-digital conversion.

The ECG, SCG, and respiratory signals were all measured simultaneously at 1000 Hz, while the subjects were in the resting supine position. In this study, only the *z*-axis component was considered for investigations.

The quality of measured signals was inspected; the data of one subject as well as one single trial of three subjects were discarded. In total, 35 remaining recordings were normalized to zero mean and unit variance.

B. Annotation, Segmentation, and Labeling

The respiration signals were examined manually to find the peaks of inhale and exhale phases. The peak of inhale (exhale) was the moment at which the inhale (exhale) ended and the exhale (inhale) phase started (see Fig. 2). Such peaks did not necessarily correspond to respiration's maxima and minima as Fig. 2 indicates (existence of multiple local maxima and minima). Therefore, a simple peak-finding algorithm was not sufficient, and visual inspection was needed. This task and its validation were performed by two experts independently to minimize the possible annotation errors.

After annotation, segmentation and labeling were undertaken. In these stages, SCGs were segmented into beat-to- beat cycles using the R-peaks of ECG signals. The Pan–Tompkins algorithm was used to detect the R-peaks of ECG [26]. Each SCG cycle was defined as the interval between two consecutive R-peaks shifted to the left (delayed) by 0.2 s and was labeled as either inhale (I) or exhale (E), based on the position of their R-peak in the respiratory cycle. The total SCG cycles were 20 373, of which, 8604 cycles were labeled as I, and 11766 were labeled as E.

C. Time and Frequency Feature Extraction, and Feature Selection

As previously mentioned, the goal was to identify the respiratory phases by analyzing the SCG cycles. Our method started with extracting informative features from time- and frequency-domain representations of SCG cycles to facilitate respiratory phase identification.

In order to have comparable features in the time domain, the number of data points in each SCG cycle was set to a fixed value. In this study, the fixed value was set at 2048, which was greater than the maximum number of data points in all cycles. To reach 2048, sufficient data points, whose value was equal to the cycle's arithmetic mean (mean-padding), were added to the end of each cycle. It should be mentioned that interpolation and extrapolation were avoided, because they would change the timings between the data points of each cycle. Such timings are correlated with cardiac events (e.g., STI), and so are vital to be left unchanged.

After the mean-padding, each SCG cycle in the time domain was divided into 512 equal-sized bins. As a result, each bin had four data points. The arithmetic mean of the data in each bin was computed and is referred to as the time-domain feature in this study. The resolution of these features in the time was 0.004 s (every 0.004 s a time-domain features was extracted).

To extract the frequency-domain features, each SCG cycle was transformed to the frequency-domain using fast Fourier transform (FFT). The first 512 FFT coefficients corresponded to the frequency range 0–500 Hz (this range was based on the sampling frequency of 1000 Hz, and the Shannon–Nyquist theorem [27]). These 512 coefficients obtained from each cycle are frequency-domain features. The resolution of these features in the frequency is $\frac{500}{512} \approx 0.98$ (every 0.98 Hz a frequency-domain features was extracted).

After extracting the time- and frequency-domain features, feature selection was done in order to select the most prominent features in identifying the respiratory phase. In this investigation, we used support vector machine (SVM), a powerful machine-learning algorithm for identification. SVM has been widely used for analyzing biomedical signals such as heart murmurs identification [28], [29], reducing false alarms during arrhythmia [30], and monitoring dental operations [31].

SVM is originally a binary identifier, which separates the data of two categories by a hyperplane found through solving a convex max–min optimization problem [32]. In order to use SVM, two steps of training and testing should be followed. In the training step, SVM uses a selective set of data (training) to develop a model. Then, in the testing step, another set of data (testing) is used to evaluate the performance of the developed model. For this study, there was no overlap between training and testing data.

If the data cannot be separated by a hyperplane in the original space, SVM transforms the data to a higher dimension using a kernel function in order to facilitate their separation. In this paper, a radial basis function (RBF) was employed as the kernel, as described by $K(X_i\ .\ X_j) = \exp(-\gamma X_i - X_j{}^2)\gamma > 0$, where X is the input vector and γ is a hyperparameter that can modify the results. SVM with RBF kernel has another hyperparameter C that controls how much misclassification is acceptable in the training stage [32]. The values of these hyperparameters were obtained using a grid search method with a fivefold cross validation [33].

To select the most prominent features, all cycles from all subjects were considered, and an SVM model was developed for each individual feature, in both time and frequency domains. The software package LIBSVM in a MATLAB platform was employed in developing the models [34]. Half of the data were randomly selected for training (uniform distribution), and the other half used for testing. The random training/testing procedure was iterated 100 times, and the total accuracy was obtained for each individual time and frequency feature. The total accuracy is the ratio of the number of correctly identified cycles to the total number of cycles (presented as a percentage). This analysis indicated which time or frequency domain features had higher accuracy in identifying the respiratory phase.

The next step in our analysis was to select the number of features that could reach the highest accuracy when combined together as the feature vector. To do this analysis, time and frequency features were considered separately and together (time frequency). These were sorted from the greatest to the smallest total accuracy. Starting from the highest accuracy feature, additional features were added one by one to form feature vectors each with a continually increasing number of features. For each feature vector, the data were randomly divided into 50% training and 50% testing groups (uniform distribution). The effect of each number of features in identifying the respiratory phases of SCG cycles was investigated using the SVM model with RBF kernel. The random training/testing procedure was iterated 100 times, and the total accuracy of each number of features was obtained.

D. Respiratory Phase Identification

After selecting the prominent features, the respiratory phase identification of SCG cycles was investigated in two training-testing scenarios: leave-one-subject-out (LOSO) and subject-specific (SS). In the LOSO scenario, the training data were selected from all subjects except the test subject (TS). In this scenario, no data from the TS were used in the training. As it was mentioned in Section II-A, two recordings were available for each subject. In the SS scenario, the training data were selected similar to LOSO, except that one recording from the TS was also considered. The testing data in this scenario were the other recording. There was no overlap between the training and testing data in either of these scenarios.

A model selection procedure was employed to choose the best model for identification. The candidate models were SVM with different nonlinear kernels, including second-order polynomial (quadratic), third-order polynomial (cubic), RBF with $\gamma = \frac{1}{2P}$ (medium Gaussian), and RBF with $\gamma = \frac{1}{32P}$ (course Gaussian), where P is the number of features.

In the LOSO scenario, each candidate model was trained with two training schemes. LOSO-Train-Scheme 1 included all SCG cycles available in the training data. To explain LOSO-Train-Scheme 2, we need to first define the "transition cycle".

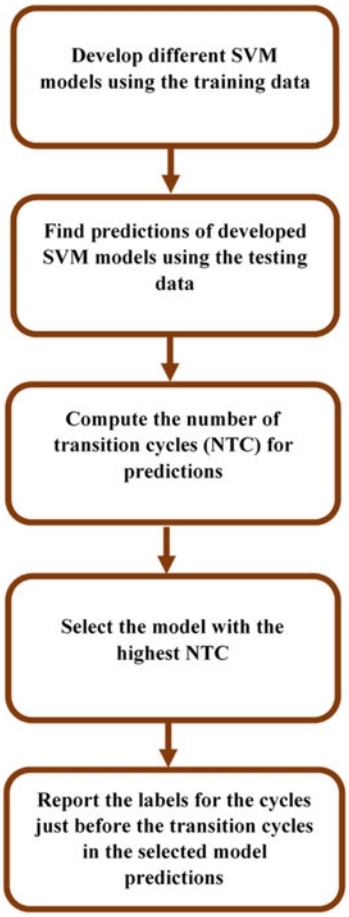

Fig. 3. Block diagram of the proposed method for identification of the respiratory phases of SCG cycles.

For each SCG signal, the i_{th} cycle (SCG_i) is a "transition cycle" if,

SCG_{i-1} = Inhale & SCG_i = Inhale & SCG_{i+1} = Exhale,

or

SCG_{i-1} = Exhale and SCG_i = Exhale and SCG_{i+1} = Inhale,

where $i = 2, 3, 4, \ldots, n$-1, and n is the total number of cycles in the SCG signal. In addition, "SCG_i = Inhale" indicates that the respiratory phase of SCG_i is inhale (a similar interpretation applies to the rest of aforesaid equations).

In this definition, SCG_i is called the "transition-cycle" because the respiration phase changes in the next cycle (SCG_{i+1}). For LOSO-Train-Scheme 2, among the training data, only the SCG cycles just before the transition-cycles (SCG_{i-1}) were selected.

Since each of the SVM models were trained in two schemes, there were a total of eight candidate models for the LOSO scenario.

In the SS scenario, there were three training schemes: SS-Train-Scheme 1, SS-Train-Scheme 2, and SS-Train-Scheme 3. The first two schemes were similar to LOSO-Train-Scheme 1 and LOSO-Train-Scheme 2, respectively. SS-Train-Scheme 3 included only the SCG cycles of the TS's recorded trial. There were a total of 12 candidate models for the SS scenario.

For each scenario, the candidate models predicted the labels of the testing data. The number of transition-cycles (NTC) was computed in the predicted labels for each model. Then, the model that had the highest NTC was selected. In the predicted labels of the selected model, only the cycles just before the transition-cycles were considered and their predicted labels were reported. Fig. 3 indicates the block diagram of the proposed method.

TABLE I
DEFINITIONS OF STATISTICAL MEASURES

Target Inhale Accuracy = 100∗ (Number of correctly identified inhale cycles/Total number of inhale cycles)
Target Exhale Accuracy = 100∗ (Number of correctly identified exhale cycles/Total number of exhale cycles)
Output Inhale Accuracy = 100∗ (Number of correctly identified inhale cycles/Total number of cycles identified as inhale)
Output Exhale Accuracy = 100∗ (Number of correctly identified exhale cycles/Total number of cycles identified as exhale)

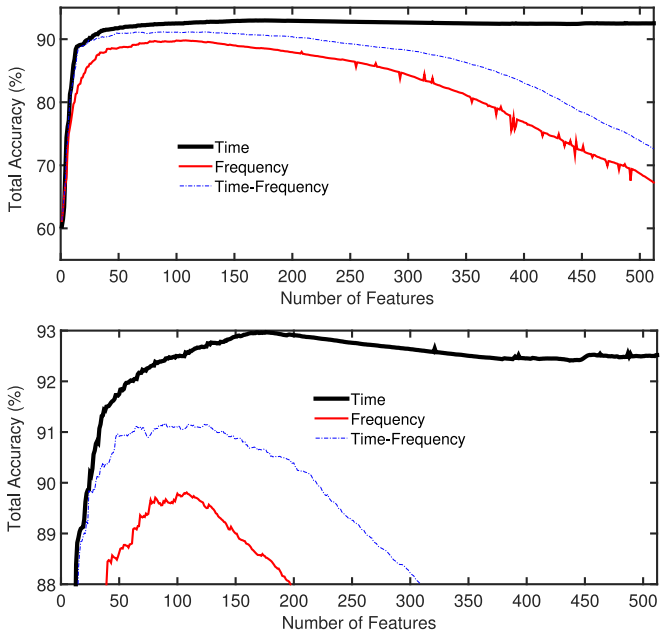

Fig. 4. (Top): effect of number of features in time, frequency, and time-frequency domains in identifying the respiratory phases of SCG cycles. (Bottom): a zoomed view of the top figure. The total accuracies of time, frequency, and time-frequency domains were ultimately decreased by increasing the number of features, each with different rates.

The performance of the proposed method in identification of the respiratory phases of SCG cycles was described by different statistical measures as defined in Table I. In this table, target data (inhale/exhale) are ground-truth labels, whereas output data (inhale/exhale) are the predictions of the selected model.

III. RESULTS

A. Feature Selection

Fig. 4 shows the effect of number of features in identifying the respiratory phases of SCG cycle for time, frequency, and time-frequency domains as described in Section II-C. According to Fig. 4, the maximum total accuracies for time, frequency, and

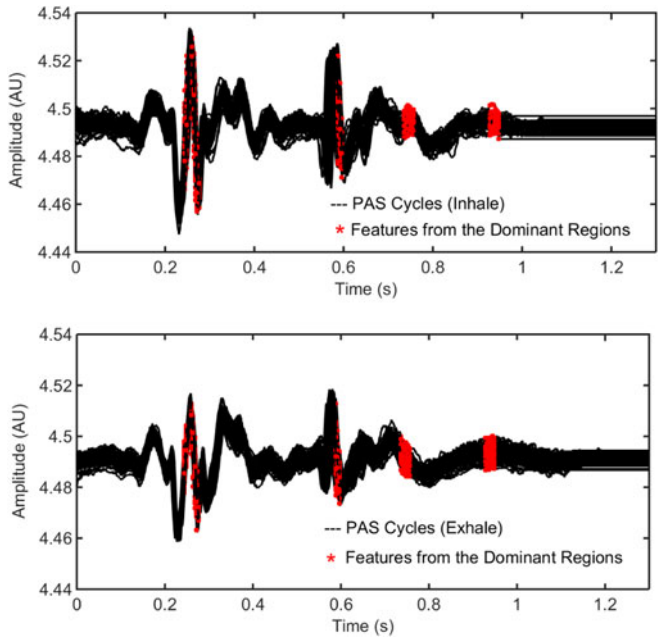

Fig. 5. Overlay plots of SCG cycles in the inhale (top) and exhale (bottom) phases obtained from one subject. The time-domain features with higher total accuracies are highlighted.

TABLE II
NUMBER OF TRANSITION CYCLES FOR DIFFERENT MODELS IN LOSO SCENARIO OBTAINED FOR ONE SUBJECT

	LOSO[a]-Train-Scheme 1				LOSO[a]-Train-Scheme 2			
	Qu[b]	Cu[c]	MG[d]	CG[e]	Qu[b]	Cu[c]	MG[d]	CG[e]
NTC[f]	308	156	279	208	328	319	363	180

[a.]: Leave one subject out
[b-e.]: Quadratic, Cubic, Medium Gaussian, Course Gaussian
[f]: Number of transition cycles

time-frequency domains were 93%, 89.8%, and 91.2%, obtained for 176, 108, and 88 selected features, respectively. The bottom plot of Fig. 4 is a zoomed view of the top plot. As we can see, the total accuracies of time, frequency, and time-frequency domains were ultimately decreased by increasing the number of features, each with different rates.

Based on this analysis, the maximum total accuracy was obtained for the selected features in the time domain. Fig. 5 highlights the time-domain features with higher total accuracies on SCG cycles in the inhale and exhale phases obtained from one subject.

B. LOSO Scenario

The respiratory phases of SCG cycles were identified in the LOSO scenario as described in Section II-D. Table II indicates the NTC of different models in this scenario obtained for one of the subjects. As Table II shows, the highest NTC was for the medium Gaussian model in LOSO-Train-Scheme 2; therefore, this model was selected. In the predicted labels of the selected model, only the cycles just before the transition cycles were considered for identification. The total accuracy of this identification for this particular subject was 91.2%. The same procedure was conducted for all subjects, and the results are shown in Table III. In this table, the average, median, and standard deviation of different statistical measures over all subjects are presented. For example, considering the total accuracy, the average, median, and standard deviation were 88.1%, 91.2%, and 11% respectively.

C. SS Scenario

The respiratory phases of SCG cycles were identified in the SS scenario. Table IV indicates NTC for different models in this scenario obtained for one recording. As Table IV shows, the highest NTC was obtained by course Gaussian model in the SS-Train-Scheme 1. This model was selected for the recording, and the total accuracy was 97.8%. Also, as can be seen, the NTC was 0 for medium Gaussian model in the SS-Train-Scheme 3, which indicates that the predicated labels were all the same and no transitions were occurred (the model was biased).

The same procedure was conducted for all recordings, and the results are shown in Table V. In this table, the average, median, and standard deviation of different statistical measures over all recordings are presented. For example, considering the total accuracy, the average, median, and standard deviation were 95.4%, 97.4%, and 7.1%, respectively.

IV. DISCUSSIONS

A. Data Collection

We used a respiration belt sensor to measure the respiration effort. To assess respiration, spirometer or impedance pneumograph are more widely used (gold standard) than a respiration belt. However, in this study, the collected belt signal was not used to assess respiration (e.g., finding apnea or breathing rate) but to label the SCG cycles into inhale and exhale. For this labeling purpose, the belt signal was accurate, reliable, and suitable.

Also, the frequency components of SCG that are correlated with respiration are mostly located in lower frequency ranges (10–40 Hz) as shown in [23]. Therefore, the accelerometer's frequency response did not affect the quality or the repeatability of our data in this study.

B. Feature Selection

The results of feature selection indicated that time features had higher accuracy compared to frequency and time-frequency features (see Fig. 4). Also, as the bottom plot of Fig. 4 shows, by adding more features, the total accuracies were first raised to a maximum value and then eventually decreased. This behavior sometimes is referred to as "peaking phenomenon" in the literature [35]. In our analysis, utilizing more features first increased the separation among inhale and exhale data; however, ultimately, because of the limited dataset size, the added features performed similarly to noise and reduced the accuracies.

Also, as seen in the bottom plot of Fig. 4, the decrement rates were different for time, frequency, and time-frequency domains. The reason for such a difference should be probably sought in the values of these features. The time-domain features were mostly nonzero, because the mean of each SCG cycle

TABLE III
DIFFERENT STATISTICAL MEASURES OBTAINED IN LOSO SCENARIO AVERAGED OVER ALL SUBJECTS

	Target Inhale Acc.[a]	Target Exhale Acc.[a]	Output Inhale Acc.[a]	Output Exhale Acc.[a]	Total Acc.[a]
Average	90.4%	87.7%	85.4%	91.4%	88.1%
Median	96.1%	88.5%	86.3%	97.1%	91.2%
Standard Deviation	14.2%	10.6%	13.8%	15.1%	11%

[a.]: Accuracy

TABLE IV
NUMBER OF TRANSITION CYCLES FOR DIFFERENT MODELS IN SS SCENARIO OBTAINED FOR ONE RECORD

	SS[a]-Train-Scheme 1				SS[a]-Train-Scheme 2				SS[a]-Train-Scheme 3			
	Qu[b]	Cu[c]	MG[d]	CG[e]	Qu[b]	Cu[c]	MG[d]	CG[e]	Qu[b]	Cu[c]	MG[d]	CG[e]
NTC[f]	135	146	174	225	151	156	198	158	15	85	0	65

[a.]: Subject specific
[b-e.]: Quadratic, Cubic, Medium Gaussian, Course Gaussian
[f.]: Number of transition cycles

TABLE V
DIFFERENT STATISTICAL MEASURES OBTAINED IN SS SCENARIO AVERAGED OVER ALL RECORDINGS

	Target Inhale Acc.[a]	Target Exhale Acc.[a]	Output Inhale Acc.[a]	Output Exhale Acc.[a]	Total Acc.[a]
Average	96.3%	93.8%	91.6%	98.3%	95.4%
Median	100%	95.8%	95.9%	100%	97.4%
Standard Deviation	10.4%	8.8%	12.6%	3%	7.1%

[a.]: Accuracy

was generally not zero. In contrast, frequency-domain features were almost zero for frequencies greater than 100 Hz. These zero-valued features did not have information for identification of inhale and exhale and, therefore, reduced the total accuracies of frequency and time-frequency domains at a faster rate as compared to the time-domain features.

The time-domain features with higher total accuracies were located in certain regions of the SCG cycle as Fig. 5 shows. Prior research has correlated cardiac events such as aortic-valve opening (AO) and aortic-valve closure (AC) to particular characteristic points on SCG [6], [8], [36]. By comparing the results depicted in Fig. 5 to these characteristic points, AO (the peak roughly between 0.2 and 0.3 s) and AC (the peak just before 0.6 s) are within the highlighted regions in Fig. 5. Another region is located after AC, in which different morphologies can be seen for inhale and exhale. The last region is particularly interesting since it is located roughly at the end of the cycle for the inhale phase (before start of the mean-padding), but on a region before the end of the cycle for the exhale. Generally, the length of SCG cycles in the exhale phase is longer than the ones in the inhale before mean-padding. Therefore, this last region is associated with the length of SCG cycle or the instantaneous heart rate.

It should be mentioned that differences in the individual instantaneous heart rate values may cause the allocation of any given feature of the SCG cycle into different bins for different subjects. This could be the case particularly for the SCG features occurring at the end of the systolic period and during the diastolic period of the cardiac cycle. This aspect may introduce unwanted noise in the identification procedure. To reduce the effect of this aspect, the length of all cycles were equalized before feature extraction using mean-padding as explained in Section II-C. Also, the proposed method involved using SVM with nonlinear kernels that transformed the data to a higher dimension to facilitate their separation. Therefore, the bins of one SCG cycle did not necessarily compare with the corresponding bins in another cycle for phase identification.

C. Respiratory Phase Identification

The selected time features were used in LOSO and SS scenarios. In LOSO, no information from the TS was used in training. However, in SS, one recording from the TS was used in training. As Tables III and V show, all the statistical measures of this scenario were improved compared to LOSO. For instance, the average total accuracy was increased from 88.1% (LOSO) to 95.4% (SS). This improvement was expected as SS could be "adjusted" accordingly with each individual subject. On the other hand, to train SS, the TS recording should be labeled as either inhale or exhale. To do this labeling, one simultaneous recording of SCG and respiration signal is needed. Such a recording can be then employed for phase identification of other SCGs that do not have respiration signals (SS scenario). Obviously, if no simultaneous recording of SCG and respiration signal is available, LOSO should be employed.

As observed, LOSO and SS scenarios identified the phase of only SCG cycles just before the transition cycles and not all cycles. Such identification cannot be considered as a limitation, as long as there exist enough SCG cycles to extract pertinent

information. For instance, in a prior study to analyze respiratory variations, the SCG signal was first subdivided into consecutive frames. Then for each frame, only the SCG cycles corresponded to the highest (exhale) and the lowest (inhale) S1 heart sound were considered for analysis [23]. Also, there is a consensus that around ten cardiac cycles are sufficient for reliably deriving STI [7] [37]. In our study, the number of identified cycles for each subject was more than 10 in both inhale and exhale phases. However, if the number of cycles is not sufficient to derive a specific cardiac parameter, the length of recording should be increased.

V. Conclusion

In this study, we developed a machine-learning method to identify the respiratory phases of SCG cycles. To select features, SCG cycles were assessed in time, frequency, and time-frequency domains. Time-domain features indicated higher total accuracies compared to other features. The time features with higher total accuracies included the characteristic points AO, AC, and the length of cardiac cycle (instantaneous heart rate). The performance of the developed method was evaluated in two training-testing scenarios: LOSO and SS. The average total identification accuracies of these scenarios were 88.1% (LOSO) and 95.4% (SS). The SS scenario resulted in better accuracies, because it could be adjusted accordingly with each individual subject.

The proposed method showed to be an efficient, reliable, and accurate approach to identify the respiratory phases of SCG cycles. The results obtained in this study establish a solid ground for future investigations to improve measurement of hemodynamic parameters, such as STI.

References

[1] D. Salerno and J. Zanetti, "Seismocardiography for monitoring changes in left ventricular function during ischemia," *CHEST J.*, vol. 100, no. 4, pp. 991–993, 1991.

[2] J. M. Zanetti and D. M. Salerno, "Seismocardiography: A technique for recording precordial acceleration," in *Proc. Annu. IEEE Symp. Comput.-Based Med. Syst.*, 1991, pp. 4–9.

[3] O. Inan *et al.*, "Ballistocardiography and seismocardiography: A review of recent advances," *IEEE J. Biomed. Heal. Informat.*, vol. 19, no. 4, pp. 1414–1427, Jul. 2015.

[4] J. M. Zanetti and K. Tavakolian, "Seismocardiography: Past, Present And Future," in *Proc. Annu. Int. Conf. IEEE Eng. Med. Biol. Soc.*, 2013, pp. 7004–7007.

[5] V. Gemignani *et al.*, "Transthoracic sensor for noninvasive assessment of left ventricular contractility: Validation in a minipig model of chronic heart failure," *Pacing Clin. Electrophysiol.*, vol. 33, no. 7, pp. 795–803, Jul. 2010.

[6] P. Bordachar *et al.*, "Validation of a new noninvasive device for the monitoring of peak endocardial acceleration in pigs: Implications for optimization of pacing site and configuration," *J. Cardiovascular Electrophysiol.*, vol. 19, no. 7, pp. 725–729, Jul. 2008.

[7] R. P. Lewis *et al.*, "A critical review of the systolic time intervals," *Circulation*, vol. 56, pp. 146–158, 1977.

[8] R. S. Crow *et al.*, "Relationship between seismocardiogram and echocardiogram for events in the cardiac cycle," *Am. J. Noninvasive Cardiol.*, vol. 8, no. 1, pp. 39–46, 1994.

[9] K. Tavakolian *et al.*, "Estimation of hemodynamic parameters from seismocardiogram," in *Proc. Comput. Cardiol.*, 2010, pp. 1055–1058.

[10] L. Giorgis *et al.*, "Analysis of cardiac micro-acceleration signals for the estimation of systolic and diastolic time intervals in cardiac resynchronization therapy," in *Proc. Comput. Cardiol.*, 2008, pp. 393–396.

[11] M. Di Rienzo *et al.*, "Wearable seismocardiography: Towards the beat-to-beat assessment of cardiac mechanics during sleep in microgravity," in *Proc. 8th Conf. Eur. Study Group Cardiovascular Oscililations*, 2014, pp. 239–240.

[12] R. P. Paiva *et al.*, "Beat-to-beat systolic time-interval measurement from heart sounds and ECG," *Physiol. Meas.*, vol. 33, no. 2, pp. 177–94, Feb. 2012.

[13] P. Carvalho *et al.*, "Comparison of systolic time interval measurement modalities for portable devices," in *Proc. Conf. IEEE Eng. Med. Biol. Soc.*, Jan. 2010, pp. 606–609.

[14] K. Pandia *et al.*, "Extracting respiratory information from seismocardiogram signals acquired on the chest using a miniature accelerometer," *Physiol. Meas.*, vol. 33, no. 10, pp. 1643–1660, Oct. 2012.

[15] T. Reinvuo *et al.*, "Measurement of respiratory rate with high-resolution accelerometer and EMFit pressure sensor," in *Proc. IEEE Sensors Appl. Symp.*, 2006, pp. 192–195.

[16] D. Sánchez Morillo *et al.*, "An accelerometer-based device for sleep apnea screening," *IEEE Trans. Inf. Technol. Biomed.*, vol. 14, no. 2, pp. 491–499, Mar. 2010.

[17] K. Tavakolian *et al.*, "Improvement of ballistocardiogram processing by inclusion of respiration information," *Physiol. Meas.*, vol. 29, pp. 771–781, 2008.

[18] P. Langley *et al.*, "Principal component analysis as a tool for analysing beat-to-beat changes in electrocardiogram features: Application to electrocardiogram derived respiration," *IEEE Trans. Biomed. Eng.*, vol. 57, no. 4, pp. 821–829, Apr. 2010.

[19] R. Bailón *et al.*, "A robust method for ECG-based estimation of the respiratory frequency during stress testing," *IEEE Trans. Biomed. Eng.*, vol. 53, no. 7, pp. 1273–1285, Jul. 2006.

[20] P. de Chazal *et al.*, "Automated processing of the single-lead electrocardiogram for the detection of obstructive sleep apnoea," *IEEE Trans. Biomed. Eng.*, vol. 50, no. 6, pp. 686–96, Jun. 2003.

[21] M. Jafari Tadi *et al.*, "Accelerometer-based method for extracting respiratory and cardiac gating information for dual gating during nuclear medicine imaging," *Int. J. Biomed. Imaging*, vol. 2014, no. 6, pp. 1–12, Jan. 2014.

[22] N. Alamdari *et al.*, "Using electromechanical signals recorded from the body for respiratory phase detection and respiratory time estimation: A comparative study," in *Proc. Comput. Cardiol. Conf.*, 2015, pp. 65–68.

[23] K. Pandia *et al.*, "A frequency domain analysis of respiratory variations in the seismocardiogram signal," in *Proc. 35th Annu. Int. Conf. IEEE Eng. Med. Biol. Soc.*, 2013, pp. 6881–6884.

[24] C. M. Bishop, *Pattern Recognition and Machine Learning*. New York, NY, USA: Springer, 2007.

[25] V. Zakeri and K. Tavakolian, "Identification of respiratory phases using seismocardiogram: A machine learning approach," in *Proc. Comput. Cardiol. Conf.*, 2015, pp. 305–308.

[26] J. Pan and W. J. Tompkins, "A real-time QRS detection algorithm," *IEEE Trans. Biomed. Eng.*, vol. BME-32, no. 3, pp. 230–236, Mar. 1985.

[27] A. V. Oppenheim and R. W. Schafer, *Discrete-Time Signal Processing*, 3rd ed. Englewood Cliffs, NJ, USA: Prentice Hall, 2009.

[28] S. Choi and Z. Jiang, "Cardiac sound murmurs classification with autoregressive spectral analysis and multi-support vector machine technique," *Comput. Biol. Med.*, vol. 40, no. 1, pp. 8–20, 2010.

[29] Z. Jiang *et al.*, "A new approach on heart murmurs classification with SVM technique," in *Proc. Int. Symp. Inform. Technol. Convergence*, 2007, pp. 240–244.

[30] J. Behar *et al.*, "ECG signal quality during arrhythmia and its application to false alarm reduction," *IEEE Trans. Biomed. Eng.*, vol. 60, no. 6, pp. 1660–1666, Jun. 2013.

[31] V. Zakeri *et al.*, "Discrimination of tooth layers and dental restorative materials using cutting sounds," *IEEE J. Biomed. Heal. Informat.*, vol. 19, no. 2, pp. 571–580, Mar. 2014.

[32] C. Cortes and V. Vapnik, "Support-vector networks," *Mach. Learn.*, vol. 20, no. 3, pp. 273–297, 1995.

[33] C. Hsu *et al.*, "A practical guide to support vector classification," Dept. Comput. Sci. Inf. Eng., Nat. Taiwan Univ., Taipei City, Taiwan, 2003.

[34] C. C. Chang and C. J. Lin, "LIBSVM: A library for support vector machines," *Trans. Intell. Syst. Technol.*, vol. 2, no. 3, pp. 27:1–27:27, 2011.

[35] C. Sima and E. R. Dougherty, "The peaking phenomenon in the presence of feature-selection," *Pattern Recognit. Lett.*, vol. 29, pp. 1667–1674, 2008.

[36] F. Khosrow-Khavar *et al.*, "Automatic annotation of seismocardiogram with high frequency precordial accelerations," *IEEE J. Biomed. Health Informat.*, vol. 19, no. 4, pp. 1428–1434, Sep. 2015.

[37] H. Boudoulas, "Systolic time intervals," *Eur. Heart J.*, vol. 11, no. suppl.I, pp. 93–104, Dec. 1990.

Authors' photographs and biographies not available at the time of publication.